

Oxygen-driven enhancement of electron correlation in hexagonal iron at Earth's inner core conditions

Bo Gyu Jang^{1,2}, Yu He¹, Ji Hoon Shim^{3,4}, Ho-kwang Mao¹, and Duck Young Kim^{1*}

¹Center for High Pressure Science and Technology Advanced Research (HPSTAR), Shanghai 201203, China.

²Korea Institute for Advanced Study, Seoul 02455, Republic of Korea

³Department of Chemistry, Pohang University of Science and Technology, Pohang 37673, Republic of Korea

⁴Division of Advanced Materials Science, Pohang University of Science and Technology, Pohang 37673, Republic of Korea

*email: duckyoung.kim@hpstar.ac.cn

Abstract

Earth's inner core consists of mainly iron with a bit of light elements. Understanding of its structure and related physical properties has been elusive for both experiment and theory due to its required extremely high pressure and temperature conditions. Here, using density functional theory plus dynamical mean field theory, we demonstrate that oxygen atoms energetically stabilize hexagonal structured iron at the inner core condition. Electrical resistivity is much enhanced compared with pure hcp-Fe, supporting the conventional thermal convection model. Moreover, our calculated seismic velocity shows a quantitative match with geologically observed Preliminary Reference Earth Model data.

The structure and composition of Earth's core have long been a question of great interest. Although iron is generally believed to be the primary component of the Earth's core, even the phase of iron is still controversial. hcp-Fe is traditionally considered as the stable phase under the inner core (IC) conditions (1). The elastic anisotropy of IC is regarded to be originated from a preferred orientation of hcp-Fe with a non-ideal c/a ratio (2). However, it was later shown that the c/a ratio of hcp-Fe becomes almost ideal at high temperature, resulting in the vanishing of the anisotropy (3, 4). An alternative scenario based on body-centered cubic (bcc) Fe was proposed (3, 5, 6), in which a diffusion mechanism at high temperatures can make bcc-Fe stable and give anisotropy (6).

The phase of iron at IC conditions is fundamentally important to model Earth's geodynamo mechanism, since the electrical properties of hcp- and bcc-Fe are known to be very different. Electronic correlations effect of transition metals, especially iron, should be considered properly at high temperature conditions (7-10) as a previous theoretical study found that the electrical conductivity from the electron-electron ($e-e$) scattering reaches ~35% of that from the electron-phonon ($e-ph$) scattering in case of hcp-Fe at Earth's core conditions (8). The electron correlation effect of bcc-Fe is much larger than that of hcp-Fe and bcc-Fe shows non-Fermi-liquid behavior (or fully incoherent behavior) at IC conditions (9). This implies that the $e-e$ scattering part can be even more significant in bcc-Fe case and therefore, the corresponding thermal conductivity should be affected by the structure of iron.

Density and velocity of IC in the Preliminary Reference Earth Model (PREM) (11) are smaller than those of pure iron. It is generally accepted that light elements should be involved to explain the density and velocity deficit of IC (12). Although several light elements, such as S, O, Si, C, and H, have been suggested (13-18), it is still a matter of debate because of the lack of direct evidence. Among those elements, oxygen has recently attracted attention as a prime candidate. The discovery of oxygen-rich iron compound, FeO₂ under deep lower mantle conditions, suggests that there is more oxygen under deep Earth conditions than we traditionally believed (19-21). Furthermore, the FeO partitioning model implied the potential existence of stable oxygen-enriched layers below the core-mantle boundary (22-24). These recent studies support that oxygen should be properly considered in the Earth's core model.

Although these light elements' effects on velocity deficit and conductivity from $e-ph$ scattering have been studied from both the experimental and theoretical sides, there has been no detailed investigation of light elements' effect on the phase of iron and conductivity from $e-e$ scattering at IC conditions. For the realistic understanding of the thermal convection of IC, however, the

contribution of light elements should be considered properly. The electrical conductivity from $e-e$ scattering (electronic correlation effect) can be sensitively affected by not only the phase of iron but also the volatiles in the compounds. Considering that iron oxides are strongly correlated compared with pure iron, the inclusion of oxygen in the IC model can modify significantly previous theoretical estimations on the thermal conductivity.

Here, we investigate the role of a small amount of oxygen on the structural and physical properties of Earth's IC. We find that Fe_xO ($x \geq 3$) can be stabilized under IC conditions using *ab initio* calculations. This series of new iron oxide has a universal hcp-Fe structure motif with intercalated oxygen atom, indicating that a small amount of oxygen can stabilize the hcp phase at IC conditions. Intercalated oxygen atoms can make covalent bonds with Fe atoms and this interaction can explain the anisotropy of the hcp phase. The existence of oxygen also enhances the electronic correlation effect compared to pure hcp-Fe. As a result, the electrical resistivity from the $e-e$ scattering part can be much enhanced, indicating that the thermal conductivity can be smaller than the previous estimation on pure iron. The density and velocity deficit of the PREM model are also well described by the existence of oxygen in the hcp-Fe motif.

We first performed structure prediction simulation of the Fe-O system at 300 GPa using the *ab initio* random structure searching (AIRSS) method based on density functional theory (DFT) calculations (Fig. 1A). We found that Fe_xO ($x \geq 3$) are on the convex hull line, showing energetic stability at IC pressure. From Fe_3O to Fe_9O , they share a common structural motif where the oxygen atom is intercalated between Fe atoms with a hcp structure, implying that X-ray diffraction (XRD) patterns of Fe_xO series can be equivalent to that of pure hcp-Fe. Fe_xO possesses $P3m1$ space group for $x=2n$ ($x > 1$) and $P\bar{6}m2$ space group for $x=2n+1$ ($x \geq 1$) (Fig. 1B), respectively. For $x=4n+1$ ($x \geq 1$), strictly speaking, it possesses $Amm2$ space group which is equivalent to a unit cell doubling of $P\bar{6}m2$ structure with a tiny distortion. The energy difference between $P\bar{6}m2$ and $Amm2$ structures is merely ~ 5 meV/f.u. for $x=5, 7, 9$. It is worth noting that our predicted crystal structures of $x=2, 3$, and 9 cases are in good agreement with previous theoretical studies (25, 26).

Standard DFT is not enough to describe the electron correlation effect of Fe 3d orbitals. While one might expect the negligible contribution of the correlation effect with pressure, several studies claimed that its effect is critical to describe the physical properties of iron even at the IC conditions (7-10). For example, previous DFT calculations predicted that a $R3m$ structure becomes the ground state of FeO at 300 GPa (25,26) but experiments data reported NiAs-type B8 phase at low temperature and CsCl-type B2 phase above 3000 K (27), clearly yielding an inconsistency.

To estimate the correlation effect of Fe 3d orbitals on the energetic stability, we performed total energy calculations and revised the convex hull using dynamical mean field theory (DMFT) calculation combined with DFT. Interestingly, DFT+DMFT calculations give an excellent match with experimental data on determining FeO phase, exhibiting the B2 phase becomes the most stable one at 300 GPa (Fig. S1). These results indicate the importance of the electron correlation effect on the physical properties of iron oxides, including the formation energy. Furthermore, we found that hcp-Fe is still energetically favorable than bcc-Fe by ~ 1 eV/f. u. (Fig. 1A), which is consistent with DFT calculations and the energy difference is unlikely to be overcome by temperature. Hexagonal Fe_xO series is on the convex hull line from Fe_3O up to hcp-Fe, indicating the stability of Fe_xO ($3 \leq x \leq 9$) under IC conditions (Fig. 1A). Thus, hexagonal-structured iron oxides are preferred in the presence of a small amount of oxygen.

As a representative example of our predicted iron oxide, figure 2A shows the crystal structure of Fe₉O. The distance between Fe atoms is aligned along the *c* direction and it is similar to that of hcp-Fe (black arrows), except for Fe atoms adjacent to the oxygen atom. The distance between Fe atoms above and below the O atom (~2.60 Å) is much shorter than the others, indicating the strong interaction between Fe and O atom. One can find that the O atom is properly screened by the nearest Fe atoms and Fe-Fe distance is fully recovered to ~ 3.40 Å of pure hcp-Fe.

d electrons occupancy of Fe atoms as a function of the distance from O atom is obtained using DFT+DMFT calculations (Fig. 2B). The numbers on Fe atoms in Fig. 2A are assigned in order of the distance from O atom, which correspond to the *y* ticks in Fig. 2B. The *d* occupancy of Fe_{*x*}O is remained to be smaller than that of hcp-Fe and it monotonically increases as *x* increases, and it eventually converges to that of hcp-Fe (the vertical dashed line). The occupancy of Fe1 atom is smaller than that of others due to the charge transferring from Fe1 atom to O atom. From the second nearest Fe atom from O atom (Fe2), the occupancy is almost recovered to pure hcp-Fe.

The partial density of state (PDOS) of Fe₉O also clearly shows the interaction between O atom and neighboring Fe atoms (Fig. 2C). The PDOS of Fe atoms in Fe_{*x*}O are remained to be similar, except for that of Fe1 atom (red line). Spectral function obtained from DFT+DMFT calculation also exhibits equivalent behavior (Fig. S2). From Fe2 atom, PDOS is almost identical to DOS of hcp-Fe, which is consistent with occupancy analysis. At the Fermi level (*E_F*), Fe1 atom has a larger density than other Fe atoms. Due to the charge transfer, Fe1 bands are shifted upward, making flat bands near the *E_F* (Fig. S2 and S3). The peak at around -11 eV observed in PDOS of both O and Fe1 atom indicates the strong hybridization between them. The crystal orbital Hamilton population (COHP) analysis between O and Fe1 atom can give insight on bonding properties (Fig. 2D) (29). The overall shape of COHP indicates covalent bonding between O and Fe1 atom, rather than just ionic bonding between them. A notable bonding state is also shown in COHP at -11 eV.

Fig. 2E shows the relative lattice constant change with respect to oxygen contents. For the direct comparison, the *c* lattice constant of each Fe_{*x*}O (*x*=5~9) compound is renormalized by the number of atoms in the unit cell along *c* direction. Due to the interaction between Fe and O atoms, *c* lattice constant is affected sensitively by the oxygen contents. The *c* lattice constant decreases ~ 5% at 10% oxygen content (*x*=9 case). *a* lattice constant is less sensitive to the oxygen content and it increases as oxygen content increases. Thus, the existence of O atoms in hcp-Fe enhances an anisotropic structural distortion not only along *c*-direction but in *ab* plane. The bonding between Fe and O atom explains the elastic anisotropy at IC. Previous studies on the pure hcp-Fe show that the *c/a* ratio becomes ideal as temperature increases (3, 4), however, the anisotropy can be induced in the presence of a small amount of oxygen. Due to the strong interaction between Fe and O, *c/a* ratio of hcp-Fe motif can be anisotropic even at high temperature. Although Fe_{*x*}O exists as polycrystal at IC condition with a globally preferred orientation, it can induce the elastic anisotropy observed in the experiment. Therefore, the existence of oxygen is an important key to understanding the elastic anisotropy at IC conditions.

Pure hcp-Fe shows a dip feature in its spectral function at the *E_F* (Fig. S2, 3). Due to the charge transfer and interaction between Fe1 and O atoms in Fe₉O, however, flat bands occur near the *E_F*. As pointed out in the previous studies (7, 9, 30), a van Hove singularity enhances the correlation strength of systems, including bcc-Fe. Flat bands near the *E_F* are well observed in Fe_{*x*}O, especially for *x* ≥ 7 (Fig. S3). In addition, Fe1-Fe1 3*d* orbitals overlap is strongly reduced

because of oxygen, making the system more incoherent. Hence, we can expect the enhanced electron correlation effect in Fe_xO compared to pure hcp-Fe.

The resistivity from electron-electron scattering, ρ_{e-e} of hcp-Fe and Fe_9O are computed with DFT+DMFT (Fig. 3A). To compare with the previously calculated result, we adopt the IC density for hcp-Fe and keep the density ratio between hcp-Fe and Fe_9O obtained from 0 K DFT calculation for Fe_9O . The calculated ρ_{e-e} of hcp-Fe well agrees with the previous theoretical studies (10). ρ_{e-e} of Fe_9O is calculated to be higher than hcp-Fe and it monotonically increases with temperature, reaching almost doubled value around 5800 K than hcp-Fe. The resistivity increasing rate of Fe_9O shows slowdown above ~ 4600 K and that of hcp-Fe keeps increasing up to 7000K. We analyzed the temperature dependence of the inverse quasiparticle lifetime Γ (Fig. 3B). Γ/kT of Fe_9O is almost converged above ~ 4600 K at which the resistivity increasing rate starts to decrease, signaling a fully incoherent regime (9, 30). For hcp-Fe case, however, the fully incoherent regime does not appear up to 7000 K. Large ρ_{e-e} (or Γ) and the reduced temperature scale of Fe_9O indicate that a small amount of oxygen enhances the electron correlation strength of hcp-Fe motif.

The total resistivity depending on the oxygen contents is shown in Fig. 3C. Diamond shapes with blue color indicate computed ρ_{e-e} using DFT+DMFT based on the structure obtained from DFT calculation at 300 GPa. The resistivity from electron-phonon scattering, ρ_{e-ph} is taken from a previous study exhibited by red squares with dashed line (31). One can notice that ρ_{e-e} and ρ_{e-ph} are both enhanced by the oxygen content and ρ_{e-e} part is more sensitively changed. Black circles with dashed line show the sum of ρ_{e-e} and ρ_{e-ph} . The resistivity of Fe_9O is $\sim 20\%$ larger than that of hcp-Fe. Considering the previously suggested oxygen portion in the Earth's core (3~6 wt%) (16), the total resistivity can increase about 20~40% compared to the pure hcp-Fe.

Oxygen effect on thermal conductivity can be estimated by assuming the linear relation between electrical conductivity, σ (ρ^{-1}) and thermal conductivity, κ (the Wiedemann-Franz law). 20~40% enhancement of resistivity leads to 17~29% reduction of thermal conductivity. Previous theoretical estimates on the thermal conductivity of pure hcp-Fe at Earth's core condition is $\kappa = 150\sim 200 \text{ W m}^{-1} \text{ K}^{-1}$ (8, 32), which is too large to explain the thermal convection in the geodynamo. Including the oxygen effect, it can be reduced to $100\sim 140 \text{ W m}^{-1} \text{ K}^{-1}$ which is consistent with a thermally convection driven dynamo (33).

Finally, we investigated the elastic properties of hcp-Fe and Fe_9O under inner core conditions. Standard DFT calculation was first adopted to verify the oxygen effect clearly. The calculated density and velocity of hcp-Fe at 300 GPa agree with the previous theoretical results. For Fe_9O , which has 3.09 wt% oxygen, the density decreases by $\sim 3.2\%$ while the compression velocity (V_p) increases by $\sim 1.9\%$ (Table S1). The electron correlation effect on the elastic properties was also verified by using DFT+DMFT calculation. The bulk modulus of hcp-Fe at 300 GPa decreases $\sim 3.4\%$ which results in $\sim 1.8\%$ reduction of seismic velocity with the assumption that the shear modulus is also reduced by the same amount. However, the thermal lattice vibration effect is dominant over the electronic correlation effect. A previous ab-initio molecular dynamics (AIMD) showed that the compression velocity decreases $\sim 11.3\%$ at 5500 K compared to the 0 K result (Table S1).

The elastic constant of hcp-Fe and Fe_9O obtained by using AIMD calculations are shown in Table S2. Our calculated elastic constants of pure hcp-Fe at 360 GPa and 6000 K has a good match with previous theoretical results (34, 35). The compression (V_p) and shear (V_s) velocities in hcp-Fe and Fe_9O are calculated with the elastic constants and compared with the PREM data (Fig. 4). As is well known, the density of pure hcp-Fe is higher than the PREM data. Fe_9O (3.09

wt% oxygen) gives much better result for density indicating the possible existence of oxygen in Earth's inner core. At 360 GPa and 6000 K, the density of Fe₉O decreases by ~3.8 % while the V_p increases by ~1.3 % compared to those of hcp-Fe, like the simple DFT results. Considering the small density difference between the PREM data and Fe₉O (330~360 GPa), there can be slightly more oxygen than 3.09 wt% which is consistent with the previous estimation (3~6 wt% oxygen) based on the seismological model (16).

References

1. S. Tateno, K. Hirose, Y. Ohishi, Y. Tatsumi, The structure of iron in Earth's inner core. *Science*. **330**, 359-361 (2010).
2. L. Stixrude, R. E. Cohen, High-pressure elasticity of iron and anisotropy of earth's inner core. *Science*. **267**, 1972-1975 (1995).
3. A. B. Belonoshko, R. Ahuja, B. Johansson, Stability of the body-centred-cubic phase of iron in the Earth's inner core. *Nature*. **424**, 1032-1034 (2003).
4. C. M. S. Gannarelli, D. Alfè, M. J. Gillan, The axial ratio of hcp iron at the conditions of the Earth's inner core. *Phys. Earth Planet. Inter.* **152**, 67-77 (2005).
5. A. B. Belonoshko, N. V. Skorodumova, A. Rosengren, B. Johansson, Elastic anisotropy of Earth's inner core. *Science*. **319**, 797-800 (2008).
6. A. B. Belonoshko, T. Lukinov, J. Fu, J. Zhao, S. Davis, S. I. Simak, Stabilization of body-centred cubic iron under inner-core conditions. *Nat. Geosci.* **10**, 312-316 (2017).
7. A. Hausoel, M. Karolak, E. Sasioglu, A. Lichtenstein, K. Held, A. Katanin, A. Toschi, G. Sangiovanni, Local magnetic moments in iron and nickel at ambient and Earth's core conditions. *Nat. Commun.* **8**, 16062-16070 (2017).
8. J. Xu, P. Zhang, K. Haule, J. Minar, S. Wimmer, H. Ebert, R. E. Cohen, Thermal conductivity and electrical resistivity of solid iron at Earth's core conditions from first principles. *Phys. Rev. Lett.* **121**, 96601-96606 (2018).
9. L. V. Pourovskii, T. Miyake, S. I. Simak, A. V. Ruban, L. Dubrovinsky, I. A. Abrikosov, Electronic properties and magnetism of iron at the Earth's inner core conditions. *Phys. Rev. B* **87**, 11530-11534 (2013).
10. L. V. Pourovskii, J. Mravlje, A. Georges, S. I. Simak, I. A. Abrikosov, Electron-electron scattering and thermal conductivity of ϵ -iron at Earth's core conditions. *New J. Phys.* **19**, 073022-073030 (2017).
11. A. M. Dziewonski, D. L. Anderson, Preliminary reference Earth model. *Phys. Earth Planet. Inter.* **25**, 297-356 (1981).
12. J.-P. Poirier, Light elements in the Earth's outer core: A critical review. *Phys. Earth Planet. Inter.* **85**, 319-337 (1994).
13. K. Tsuno, D. J. Frost, D. C. Rubie, Simultaneous partitioning of silicon and oxygen into the Earth's core during early Earth differentiation. *Geophys. Res. Lett.* **40**, 66-71 (2013).
14. H. Huang, Y. Fei, L. Cai, F. Jing, X. Hu, H. Xie, L. Zhang, Z. Gong, Evidence for an oxygen-depleted liquid outer core of the Earth. *Nature*. **479**, 513-516 (2011).

15. Z. Mao, J. F. Lin, J. Liu, A. Alatas, L. Gao, J. Zhao, H. K. Mao, Sound velocities of Fe and Fe-Si alloy in the Earth's core. *Proc. Natl. Acad. Sci. U. S. A.* **109**, 10239–10244 (2012).
16. J. Badro, A. S. Côté, J. P. Brodholt, A seismologically consistent compositional model of Earth's core. *Proc. Natl. Acad. Sci. U. S. A.* **111**, 7542–7545 (2014).
17. T. Sakamaki, E. Ohtani, H. Fukui, S. Kamada, S. Takahashi, T. Sakairi, A. Takahata, T. Sakai, S. Tsutsui, D. Ishikawa, R. Shiraishi, Y. Seto, T. Tsuchiya, A. Q. R. Baron, Constraints on earth's inner core composition inferred from measurements of the sound velocity of hcp-iron in extreme conditions. *Sci. Adv.* **2**, e1500802 (2016).
18. Y. Zhang, T. Sekine, H. He, Y. Yu, F. Liu, M. Zhang, Experimental constraints on light elements in the Earth's outer core. *Sci. Rep.* **6**, 22473–22481 (2016).
19. Q. Hu, D. Y. Kim, W. Yang, L. Yang, Y. Meng, L. Zhang, H.-K. Mao, FeO₂ and FeOOH under deep lower-mantle conditions and Earth's oxygen–hydrogen cycles. *Nature.* **534**, 241–244 (2016).
20. J. Liu, Q. Hu, D. Young Kim, Z. Wu, W. Wang, Y. Xiao, P. Chow, Y. Meng, V. B. Prakapenka, H. K. Mao, W. L. Mao, Hydrogen-bearing iron peroxide and the origin of ultralow-velocity zones. *Nature.* **551**, 494–497 (2017).
21. J. Liu, Q. Hu, W. Bi, L. Yang, Y. Xiao, P. Chow, Y. Meng, V. B. Prakapenka, H.-K. Mao, W. L. Mao, Altered chemistry of oxygen and iron under deep Earth conditions. *Nat. Commun.* **10**, 153 (2019).
22. A. Shahar, E. A. Schauble, R. Caracas, A. E. Gleason, M. M. Reagan, Y. Xiao, J. Shu, W. Mao, Pressure-dependent isotropic composition of iron alloys. *Science* **352**, 580–582 (2016).
23. M. Pozzo, C. Davies, D. Gubbins, D. Alfè, FeO content of Earth's liquid core. *Phys. Rev. X.* **9**, 041018–041032 (2019).
24. C. J. Davies, M. Pozzo, D. Gubbins, D. Alfè, Transfer of oxygen to Earth's core from a long-lived magma ocean. *Earth Planet. Sci. Lett.* **538**, 116208–116218 (2020).
25. S. Huang, X. Wu, S. Qin, Stability and anisotropy of (Fe_xNi_{1-x})₂O under high pressure and implications in Earth's and super-Earths' core. *Sci. Rep.* **8**, 236 (2018).
26. G. L. Weerasinghe, C. J. Pickard, R. J. Needs, Computational searches for iron oxides at high pressures. *J. Phys. Condens. Matter.* **27**, 455501–455509 (2015).
27. H. Ozawa, F. Takahashi, K. Hirose, Y. Ohishi, N. Hirao, Phase transition of FeO and stratification in earth's outer core. *Science.* **334**, 792–794 (2011).
28. K. Ohta, R. E. Cohen, K. Hirose, K. Haule, K. Shimizu, Y. Ohishi, Experimental and theoretical evidence for pressure-induced metallization in FeO with rocksalt-type structure. *Phys. Rev. Lett.* **106**, 026403–026407 (2011).
29. R. Nelson, C. Ertural, J. George, V. L. Deringer, G. Hautier, R. Dronskowski, LOBSTER: Local orbital projections, atomic charges, and chemical-bonding analysis from projector-augmented-wave-based density-functional theory, *J Comput Chem.* **41**, 1931–1940 (2020).
30. J. Mravlje, M. Aichhorn, T. Miyake, K. Haule, G. Kotliar, A. Georges, Coherence-incoherence crossover and the mass-renormalization puzzles in Sr₂RuO₄. *Phys. Rev. Lett.* **106**, 096401–096404 (2011).

31. N. De Koker, G. Steinle-Neumann, V. Vlček, Electrical resistivity and thermal conductivity of liquid Fe alloys at high P and T, and heat flux in Earth's core. *Proc. Natl. Acad. Sci. U. S. A.* **109**, 4070–4073 (2012).
32. L. V. Pourovskii, J. Mravlje, M. Pozzo, D. Alfè, Electronic correlations and transport in iron at Earth's core conditions. *Nat. Commun.* **11**, 4105-4112 (2020).
33. P. Driscoll, D. Bercovici, On the thermal and magnetic histories of Earth and Venus: Influences of melting, radioactivity, and conductivity. *Phys. Earth Planet. Inter.* **236**, 36–51 (2014).
34. B. Martorell, L. Vocadlo, J. Brodholt, I. G. Wood, Strong Premelting Effect in the Elastic Properties of hcp-Fe Under Inner-Core Conditions. *Science.* **342**, 466–468 (2013).
35. Y. Li, L. Vočadlo, J. P. Brodholt, The elastic properties of hcp-Fe alloys under the conditions of the Earth's inner core. *Earth Planet. Sci. Lett.* **493**, 118–127 (2018).
36. K. Haule, C-H. Yee, K. Kim, Dynamical mean-field theory within the full-potential methods: electronic structure of CeIrIn₅, CeCoIn₅, and CeRhIn₅. *Phys. Rev. B* **81**, 195107-195136 (2010).
37. P. Blaha, K. Schwarz, G. K. H. Madsen, D. Kvasnicka, J. Luitz, R. Laskowski, F. Tran, and L. D. Marks, *WIEN2k, An Augmented Plane Wave + Local Orbitals Program for Calculating Crystal Properties* (Karlheinz Schwarz, Techn. Universität Wien, Austria, 2018).
38. J. P. Perdew, K. Burke, M. Ernzerhof, Generalized gradient approximation made simple. *Phys. Rev. Lett.* **77**, 3865-3868 (1996).
39. K. Haule, Exact double counting in combining the dynamical mean field theory and the density functional theory. *Phys. Rev. Lett.* **115**, 196403-196407 (2015).
40. K. Haule, Quantum Monte Carlo impurity solver for cluster dynamical mean-field and electronic structure calculations with adjustable cluster base. *Phys. Rev. B* **75**, 155113-155124 (2007).
41. L. Vočadlo, D. P. Dobson, I. G. Wood, Ab initio calculations of the elasticity of hcp-Fe as a function of temperature at inner-core pressure. *Earth Planet. Sci. Lett.* **288**, 534–538 (2009).

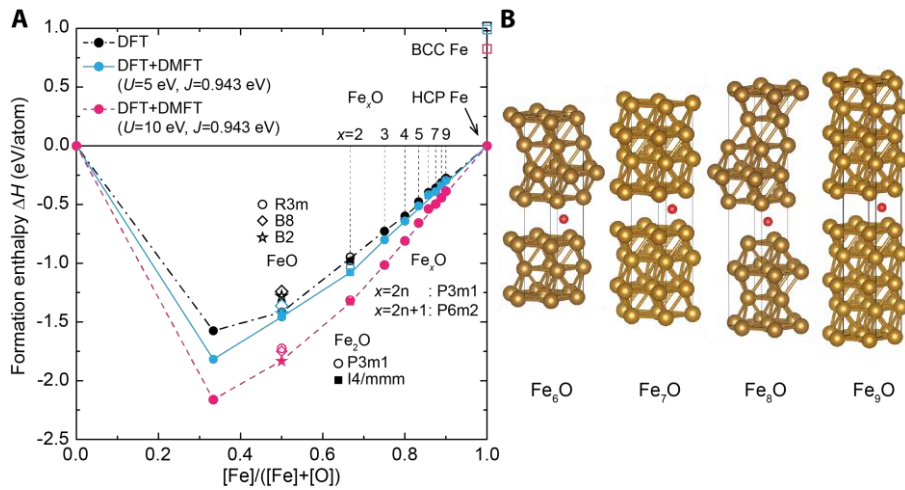


Fig. 1. Crystal structure prediction of Fe_xO at the IC conditions. (A) Convex hull plot for Fe-O system with the horizontal decomposition line into O and Fe. To verify the electron correlation effect on the formation energy, DFT+DMFT calculation was also employed. (B) Universal hexagonal crystal structure of Fe_xO ($x \geq 3$). Fe_xO can be understood as oxygen intercalated hcp-Fe. The small amount of oxygen can stabilize the hexagonal structure of Fe.

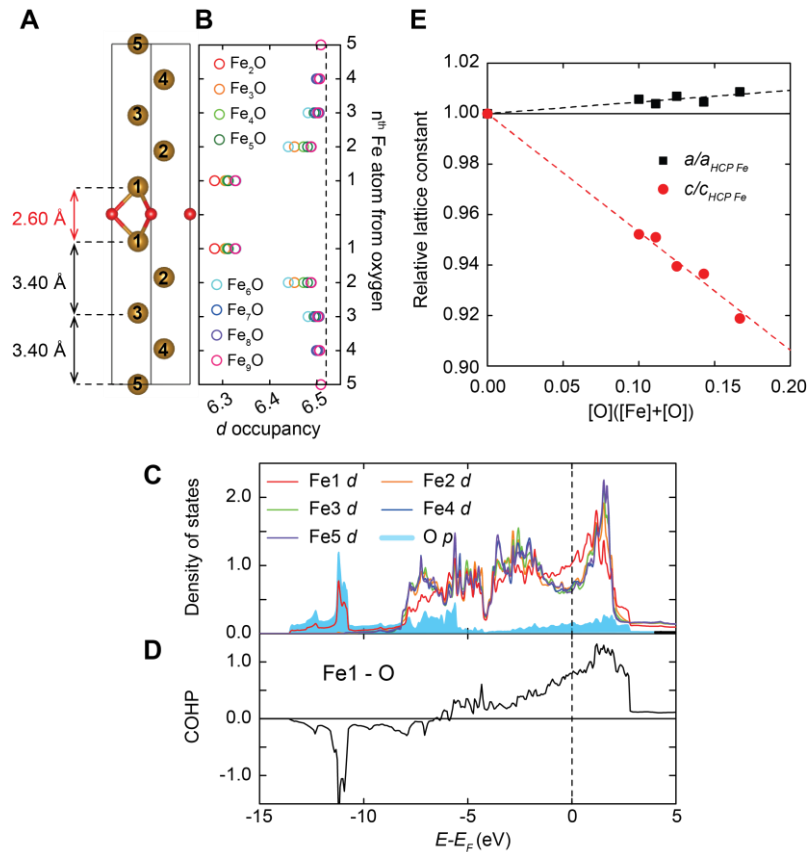


Fig. 2. Bonding properties between Fe and O atoms. (A) Crystal structure of Fe_9O at 300 GPa. The bond length between Fe atoms above and below oxygen atom (Fe1-Fe1; red arrow) is shorter than the bond length between the second nearest Fe atoms (eg., Fe1-Fe3 or Fe3-Fe5; black arrows) (B) d electron occupancy of Fe obtained from DFT+DMFT calculation. Due to the charge transfer from Fe1 to oxygen atom, d occupancy of Fe1 atom is smaller than those of other Fe atoms (C) Partial density of states (PDOS) of Fe_9O . PDOSs of Fe2-Fe5 show a dip feature at the E_F like pure hcp-Fe, while PDOS of Fe1 shows larger DOS at the E_F . (D) Crystal orbital Hamilton population (COHP) analysis between O and Fe1 atom. (E) Relative lattice constant depending on oxygen contents. The c axis becomes shorter as oxygen contents increases.

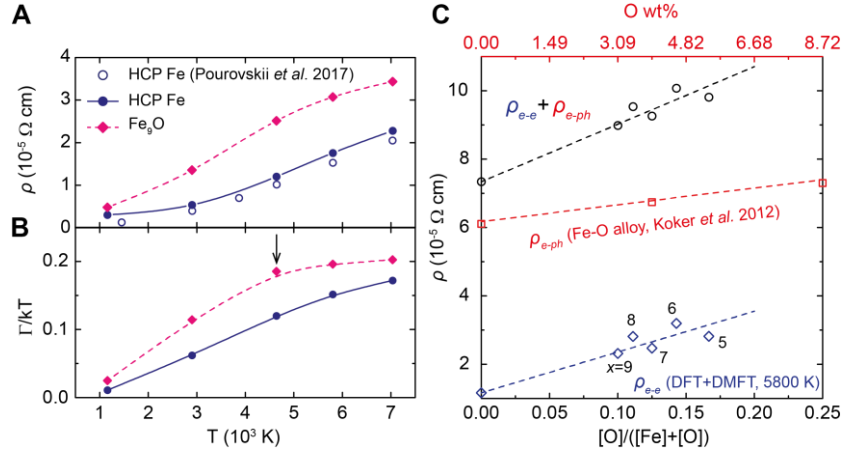


Fig. 3. Resistivity of Fe_xO. (A) Resistivity from e - e scattering part (ρ_{e-e}) from DFT+DMFT calculations. Our calculated result of hcp-Fe well agrees with the previous results. ρ_{e-e} of Fe₉O is much higher than that of pure hcp-Fe. (B) Inverse quasiparticle lifetime Γ of hcp-Fe and Fe₉O. Γ/kT of hcp-Fe shows almost T linear behavior up to 7000 K, while that of Fe₉O is almost saturated at $\sim 4600 \text{ K}$. (C) Total resistivity ($\rho_{e-e} + \rho_{e-ph}$) depending on oxygen contents. ρ_{e-ph} is taken from the previous studies. Although ρ_{e-e} and ρ_{e-ph} both increase as oxygen contents increase, ρ_{e-e} is more sensitively affected by oxygen contents.

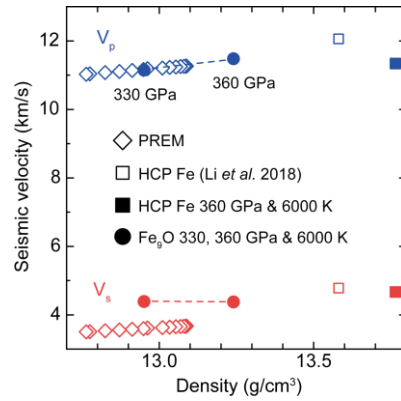


Fig. 4. Seismic velocity of hcp-Fe and Fe_9O . Diamond, square, and circle points indicate the seismic velocity of PREM, hcp-Fe, and Fe_9O , respectively. The density and velocity of pure hcp-Fe at 360 GPa is too high compared to the PREM data. For Fe_9O case, a small amount of oxygen suppresses the density and velocity, resulting in better agreement with RREM data.